CHAPTER 73

SECOND-ORDER INTERACTION BETWEEN RANDOM WAVE AND SUBMERGED OBSTACLE

Akinori Yoshida[1], Keisuke Murakami,[2]
Masaru Yamashiro[3], Haruyuki Kojima[4]

Abstruct

A numerical method to solve the second-order interaction between a multi-component random wave and a submerged obstacle is presented by using Stokes' wave expansion and Green's second identity. The wave is unidirectional random wave, but nonlinear interaction up to the second-order is strictly considered. Laboratory experiments with several multicomponent random waves for several different wave powers are conducted. The transmitted wave spectra obtained both in the experiment and in the numerical calculation are compared. The effects of wave breaking on the obstacle to the transmitted wave spectra are also investigated.

Introduction

When propagating waves encounter a submerged obstacle, comparably large amplitude of higher order waves (free waves) could be generated because of the abruptly decreased water depth and nonlinear free-surface boundary condition. This free wave generation is called near-resonant interaction (e.g., Bryand, 1973). Several numerical method applicable to solve this nonlinear wave-structure interaction have been presented: for example, Massel(1983) solved the second-order interaction for a submerged step using the method of matched eigenfunction expansions; Ohyama and Nadaoka (1992) investigated nonlinear interaction for a submerged dike using time domain boundary integral

[1]Associate Professor, Dept. of Civil Eng., Kyushu Univ., Hakozaki, Higashi-ku, Fukuoka 812, Japan
[2]Reearch Associate, ditto
[3]Graduate student, ditto
[4]Professor, Dept. of Civil Eng., Kyushu Kyoritsu Univ., Yahatanishi-ku, Kitakyushu, 807, Japan

equation method; Kojima et al.(1994) clarified the second-order interaction for a submerged horizontal plate using the collocation methd of matched eigenfunction expansions; Yoshida. et al.(1994) solved the second-order interaction between bichromatic wave and submerged structure using a frequency domain boundary integral equation method.

These solutions however deal mostly with interaction of a single frequency component wave. Since in real sea state waves generally consist of a multicomponent wave of different frequency, second-order interactions between different frequency components also occur, and lower and higher harmonics at the difference and the sum frequencies of the primary component waves are generated. The knowledge of this energy transfer between frequencies caused by nonlinear wave-structure interactions seems to be lacking.

Main aim of this study is to obtain a theoretical method to solve interaction problems between a random wave train of arbitrary spectrum and a submerged obstacle in relatively deep water depth. The wave is an unidirectional random wave, but nonlinear interaction up to the second-order is strictly considered. A solution to a multicomponent random wave is first derived using frequency domain boundary integral equation method, then Laboratory experiments with several multicomponent random waves are conducted as well as numerical calculations. Transmitted wave spectra obtained in the experiment are compared to those obtained with the present method. The effect of wave breaking on the obstacle to the free-wave generation is also investigated.

Theoretical Formulation

Basic assumptions and free surface boundary condition

As shown in figure-1, a N component random wave is incident on a submerged obstacle from the positive x-direction. The water depth h is constant, and the angular frequency of each component wave is designated with σ_p, $(p = 1, \cdots, N)$. Fluid motion is assumed to be incompressible, inviscid wave motion, and the velocity potential $\Phi(x, z, t)$ exists. We consider the waves are Stokes' waves, and the velocity potential $\Phi(x, z, t)$, water surface variation $\zeta(x, t)$, Bernoulli's constant $Q(t)$ can be expanded with small parameter $\epsilon(= k\zeta_0)$ as follows:

$$\Phi(x,z,t) = \frac{g\zeta_0}{\sigma}\left\{\epsilon\varphi^{(1)}(x,z,t) + \epsilon^2\varphi^{(2)}(x,z,t) + \cdots\right\} \tag{1}$$

$$\zeta(x,t) = \zeta_0\left\{\zeta^{(1)}(x,t) + \epsilon\zeta^{(2)}(x,t) + \cdots\right\} \tag{2}$$

$$Q(t) = g\zeta_0\left\{Q^{(1)}(t) + \epsilon Q^{(2)}(t) + \cdots\right\} \tag{3}$$

in which k, σ, ζ_0 mean the wave number, the angular frequency and the wave amplitude, respectively, of a characteristic wave in the multicomponent random wave.

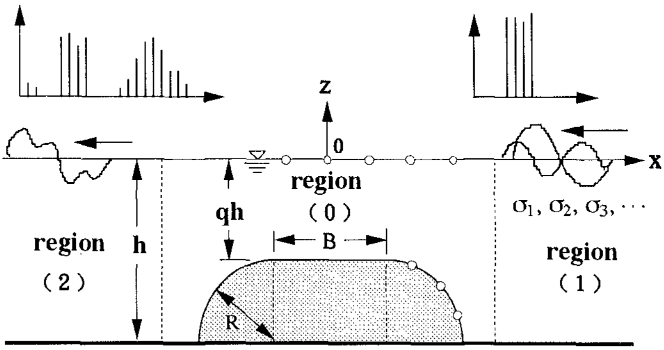

Figure 1: Definition sketch

From Stokes' wave theory, the free surface boundary condition for the second-order velocity potential $\varphi^{(2)}$ can be expressed in terms of the first-order velocity potential $\varphi^{(1)}$ as (e.g. Newman,1977)

$$\frac{\partial\varphi^{(2)}}{\partial z}+\frac{1}{g}\frac{\partial^2\varphi^{(2)}}{\partial t^2}=-\frac{1}{k\sigma}\frac{\partial}{\partial t}\left\{\left(\frac{\partial\varphi^{(1)}}{\partial x}\right)^2+\left(\frac{\partial\varphi^{(1)}}{\partial z}\right)^2\right\}$$
$$-\frac{1}{kg\sigma}\frac{\partial\varphi^{(1)}}{\partial t}\frac{\partial}{\partial z}\left\{\frac{\partial^2\varphi^{(1)}}{\partial t^2}+g\frac{\partial\varphi^{(1)}}{\partial z}\right\}+\frac{\sigma}{g}\frac{\partial Q^{(2)}(t)}{\partial t} \tag{4}$$

The first-order velocity potential $\varphi^{(1)}(x,z,t)$ can be expressed as

$$\varphi^{(1)}(x,z,t)=Re\left[\sum_{p=1}^{N}\phi_p(x,z)e^{i\sigma_p t}\right] \tag{5}$$

where $\phi_p(x,z)$ is a non-dimensional complex function.

Substituting equation (5) into equation (4), we have

$$\frac{\partial\varphi^{(2)}}{\partial z}+\frac{1}{g}\frac{\partial^2\varphi^{(2)}}{\partial t^2}-\frac{\sigma}{g}\frac{\partial Q^{(2)}}{\partial t}$$
$$=Re\left[\sum_{p=1}^{N}\left\{\Omega_{pp}(x)e^{i\sigma_{pp}t}+\Pi_{pp}(x)\right\}\right.$$
$$\left.+\sum_{p=1}^{N}\sum_{q=p+1}^{N}\left\{\Omega_{pq}(x)e^{i\sigma_{pq}t}+\overline{\Omega}_{pq}(x)e^{i\overline{\sigma}_{pq}t}\right\}\right] \tag{6}$$

where $\Omega_{pp}(x)$, $\Omega_{pq}(x)$, $\overline{\Omega}_{pq}(x)$ and $\Pi_{pp}(x)$ are given by

$$\Omega_{pp}(x)=-\frac{i}{2k}\left[\frac{\sigma_{pp}}{\sigma}\left\{\left(\frac{\partial\phi_p}{\partial x}\right)^2+\left(\frac{\partial\phi_p}{\partial z}\right)^2\right\}+\frac{\sigma_p}{\sigma}\phi_p\left\{\frac{{\sigma_p}^2}{g}\frac{\partial\phi_p}{\partial z}-\frac{\partial^2\phi_p}{\partial z^2}\right\}\right]_{z=0} \tag{7}$$

$$\left.\begin{aligned}\Omega_{pq}(x) = -\frac{i}{2k}\Bigg[&2\frac{\sigma_{pq}}{\sigma}\left\{\frac{\partial\phi_p}{\partial x}\frac{\partial\phi_q}{\partial x}+\frac{\partial\phi_p}{\partial z}\frac{\partial\phi_q}{\partial z}\right\}\\&+\frac{\sigma_p}{\sigma}\phi_p\left\{\frac{\sigma_q^2}{g}\frac{\partial\phi_q}{\partial z}-\frac{\partial^2\phi_q}{\partial z^2}\right\}+\frac{\sigma_q}{\sigma}\phi_q\left\{\frac{\sigma_p^2}{g}\frac{\partial\phi_p}{\partial z}-\frac{\partial^2\phi_p}{\partial z^2}\right\}\Bigg]_{z=0}\end{aligned}\right\} \tag{8}$$

$$\left.\begin{aligned}\overline{\Omega}_{pq}(x) = -\frac{i}{2k}\Bigg[&2\frac{\overline{\sigma}_{pq}}{\sigma}\left\{\frac{\partial\phi_p}{\partial x}\overline{\frac{\partial\phi_q}{\partial x}}+\frac{\partial\phi_p}{\partial z}\overline{\frac{\partial\phi_q}{\partial z}}\right\}\\&+\frac{\sigma_p}{\sigma}\phi_p\left\{\frac{\sigma_q^2}{g}\overline{\frac{\partial\phi_q}{\partial z}}-\overline{\frac{\partial^2\phi_q}{\partial z^2}}\right\}-\frac{\sigma_q}{\sigma}\overline{\phi_q}\left\{\frac{\sigma_p^2}{g}\frac{\partial\phi_p}{\partial z}-\frac{\partial^2\phi_p}{\partial z^2}\right\}\Bigg]_{z=0}\end{aligned}\right\} \tag{9}$$

$$\Pi_{pp}(x) = -\frac{i}{2k}\left[\frac{\sigma_p}{\sigma}\phi_p\left\{\frac{\sigma_p^2}{g}\overline{\frac{\partial\phi_p}{\partial z}}-\overline{\frac{\partial^2\phi_p}{\partial z^2}}\right\}\right]_{z=0} \tag{10}$$

in which $\overline{\phi_q}$, $\overline{\partial\phi_p/\partial z}, \cdots$ mean complex conjugate of ϕ_q, $\partial\phi_p/\partial z, \cdots$, and σ_{pp}, σ_{pq}, $\overline{\sigma}_{pq}$ mean angular frequencies defined by $\sigma_{pp} = 2\sigma_p$, $\sigma_{pq} = \sigma_p + \sigma_q$, $\overline{\sigma}_{pq} = \sigma_p - \sigma_q$

Equation (6) implys the second-order porential $\varphi^{(2)}$ takes the form as

$$\begin{aligned}\varphi^{(2)}(x,z,t) = Re\Bigg[&\sum_{p=1}^{N}\left\{\phi_{0pp}^{(2)}(x,z)+\phi_{pp}^{(2)}(x,z)e^{i\sigma_{pp}t}\right\}\\&+\sum_{p=1}^{N}\sum_{q=p+1}^{N}\left\{\phi_{pq}^{(2)}(x,z)e^{i\sigma_{pq}t}+\phi_{pq*}^{(2)}(x,z)e^{i\overline{\sigma}_{pq}t}\right\}\Bigg]\end{aligned} \tag{11}$$

where $\phi_{0pp}^{(2)}(x,z)$, $\phi_{pp}^{(2)}(x,z), \cdots$, are non-dimensional complex functions; the stationary component $\phi_{0pp}^{(2)}(x,z)$ does not contribute to the estimation of the second-order water surface variation and the pressure of the fluid motion, thus it will be neglected in the theoretical formulation from now on.

Then from equation (11) and equation (6), the free surface boundary conditions for $\phi_{pp}^{(2)}$, $\phi_{pq}^{(2)}$ and $\phi_{pq*}^{(2)}$ are obtained, for example, for $\phi_{pp}^{(2)}$ as

$$\frac{\partial\phi_{pp}^{(2)}}{\partial z}-\frac{{\sigma_{pp}}^2}{g}\phi_{pp}^{(2)} = \Omega_{pp}(x) \tag{12}$$

Exact solutions in the open regions (1) and (2)

The first-order potential functions ϕ_p in the open region (1) and (2) are found in any textbook and they can be expressed as:

$$\phi_p(x,z) = \begin{cases}\left\{a_pe^{ik_px}+A_pe^{-ik_px}\right\}Z(k_p,z) & (\text{region(1)})\\ \left\{B_pe^{ik_px}\right\}Z(k_p,z) & (\text{region(2)})\end{cases} \tag{13}$$

in which $Z(k_p, z) = \cosh k_p(z+h)/\cosh k_p h$ and k_p is the wave number given by the dispersion equation, $\sigma_p^2/g = k_p \tanh k_p h$.

The complex coefficient a_p denotes the wave amplitude and phase of each component of the incident wave, with angular frequency σ_p; the complex coefficients A_p and B_p, the wave amplitude and phase of each component of the reflected and transmitted waves, respectively.

Substitution of the first-order potential into equations (7), (8) and (9) yields

$$\Omega_{pp}(x) = \begin{cases} -i\beta_1 \left\{ a_p^2 e^{ik_{pp}x} + A_p^2 e^{-ik_{pp}x} \right\} - i\beta_2 a_p A_p & \text{(region(1))} \\ -i\beta_1 B_p e^{ik_{pp}x} & \text{(region(2))} \end{cases} \tag{14}$$

$$\Omega_{pq}(x) = \begin{cases} -i\beta_3 \left\{ a_p a_q e^{ik_{pq}x} + A_p A_q e^{-ik_{pq}x} \right\} & \\ \qquad -i\beta_4 \left\{ a_p A_q e^{i\overline{k}_{pq}x} + a_q A_p e^{-i\overline{k}_{pq}x} \right\} & \text{(region(1))} \\ -i\beta_3 B_p B_q e^{ik_{pq}x} & \text{(region(2))} \end{cases} \tag{15}$$

$$\overline{\Omega}_{pq}(x) = \begin{cases} -i\beta_5 \left\{ a_p \overline{a_q} e^{i\overline{k}_{pq}x} + A_p \overline{A_q} e^{-i\overline{k}_{pq}x} \right\} & \\ \qquad -i\beta_6 \left\{ a_p \overline{A_q} e^{ik_{pq}x} + \overline{a_q} A_p e^{-ik_{pq}x} \right\} & \text{(region(1))} \\ -i\beta_5 B_p \overline{B_q} e^{i\overline{k}_{pq}x} & \text{(region(2))} \end{cases} \tag{16}$$

in which $k_{pp} = k_p + k_p$, $k_{pq} = k_p + k_q$, $\overline{k}_{pq} = |k_p - k_q|$, $\Gamma_p = {\sigma_p}^2/g$ and β_1, $\beta_2, \cdots$ are

$$\left.\begin{aligned}
\beta_1 &= \frac{3}{2k}\frac{\sigma_p}{\sigma}\left\{\Gamma_p^2 - k_p^2\right\}, \qquad \beta_2 = \frac{1}{k}\frac{\sigma_p}{\sigma}\left\{3\Gamma_p^2 + k_p^2\right\} \\
\beta_3 &= \frac{1}{2k}\left[2\frac{\sigma_{pq}}{\sigma}\left\{\Gamma_p\Gamma_q - k_p k_q\right\} + \frac{\sigma_p}{\sigma}\left\{\Gamma_q^2 - k_q^2\right\} + \frac{\sigma_q}{\sigma}\left\{\Gamma_p^2 - k_p^2\right\}\right] \\
\beta_4 &= \frac{1}{2k}\left[2\frac{\sigma_{pq}}{\sigma}\left\{\Gamma_p\Gamma_q + k_p k_q\right\} + \frac{\sigma_p}{\sigma}\left\{\Gamma_q^2 - k_q^2\right\} + \frac{\sigma_q}{\sigma}\left\{\Gamma_p^2 - k_p^2\right\}\right] \\
\beta_5 &= \frac{1}{2k}\left[2\frac{\overline{\sigma}_{pq}}{\sigma}\left\{\Gamma_p\Gamma_q + k_p k_q\right\} + \frac{\sigma_p}{\sigma}\left\{\Gamma_q^2 - k_q^2\right\} - \frac{\sigma_q}{\sigma}\left\{\Gamma_p^2 - k_p^2\right\}\right] \\
\beta_6 &= \frac{1}{2k}\left[2\frac{\overline{\sigma}_{pq}}{\sigma}\left\{\Gamma_p\Gamma_q - k_p k_q\right\} + \frac{\sigma_p}{\sigma}\left\{\Gamma_q^2 - k_q^2\right\} - \frac{\sigma_q}{\sigma}\left\{\Gamma_p^2 - k_p^2\right\}\right]
\end{aligned}\right\}$$

Now we can derive a general solution of the second-order potential function in the open region (1) and (2). The equations, for example, governing $\phi_{pp}^{(2)}$ can be given by

$$\frac{\partial^2 \phi_{pp}^{(2)}}{\partial x^2} + \frac{\partial^2 \phi_{pp}^{(2)}}{\partial z^2} = 0 \qquad (-h \leq z \leq 0) \tag{17}$$

$$\frac{\partial \phi_{pp}^{(2)}}{\partial z} = 0 \qquad (z = -h) \tag{18}$$

$$\frac{\partial \phi_{pp}^{(2)}}{\partial z} - \frac{{\sigma_{pp}}^2}{g}\phi_{pp}^{(2)} = -i\beta_1 \left\{ a_p^2 e^{ik_{pp}x} + A_p^2 e^{-ik_{pp}x} \right\} - i\beta_2 a_p A_p \qquad (z = 0) \tag{19}$$

The general solution $\phi_{pp}^{(2)}$ can be obtained by the sum of a homogeneous solution which satisfies homogeneous surface boundary condition given by replacing the right-hand side of equation (19) by zero and a special solution which satisfies equation (19), and it can be obtained, after some calculations, as

$$\left. \begin{aligned} \phi_{pp}^{(2)}(x,z) = {} & A_{pp}^{(2)} Z(k_{pp}^{(2)}, z) e^{-ik_{pp}^{(2)}x} + ib_{s1} a_p A_p \\ & + ia_{s1} \left\{ a_p^2 e^{ik_{pp}x} + A_p^2 e^{-ik_{pp}x} \right\} Z(k_{pp}, z) \end{aligned} \right\} \tag{20}$$

and similarly $\phi_{pq}^{(2)}$ and $\phi_{pq*}^{(2)}$ are also obtained as:

$$\left. \begin{aligned} \phi_{pq}^{(2)}(x,z) = {} & A_{pq}^{(2)} Z(k_{pq}^{(2)}, z) e^{-ik_{pq}^{(2)}x} \\ & + ic_{s1} \left\{ a_p a_q e^{ik_{pq}x} + A_p A_q e^{-ik_{pq}x} \right\} Z(k_{pq}, z) \\ & + id_{s1} \left\{ a_p A_q e^{i\overline{k}_{pq}x} + A_p a_q e^{-i\overline{k}_{pq}x} \right\} Z(\overline{k}_{pq}, z) \end{aligned} \right\} \tag{21}$$

$$\left. \begin{aligned} \phi_{pq*}^{(2)}(x,z) = {} & A_{pq*}^{(2)} Z(k_{pq*}^{(2)}, z) e^{-ik_{pq*}^{(2)}x} \\ & + id_{s2} \left\{ a_p \overline{a_q} e^{i\overline{k}_{pq}x} + A_p \overline{A_q} e^{-i\overline{k}_{pq}x} \right\} Z(\overline{k}_{pq}, z) \\ & + ic_{s2} \left\{ a_p \overline{A_q} e^{ik_{pq}x} + A_p \overline{a_q} e^{-ik_{pq}x} \right\} Z(k_{pq}, z) \end{aligned} \right\} \tag{22}$$

in which $k_{pp}^{(2)}$, $k_{pq}^{(2)}$ and $k_{pq*}^{(2)}$ are the wave numbers given by the dispersion equations to angular frequencies, σ_{pp}, σ_{pq} and $\overline{\sigma}_{pq}$, respectively. The coefficients a_{s1}, $b_{s1}, \cdots$ are

$$\left. \begin{aligned} a_{s1} &= \frac{-\beta_1}{k_{pp}\tanh k_{pp}h - \Gamma_{pp}}, & b_{s1} &= \frac{\beta_2}{\Gamma_{pp}} \\ c_{s1} &= \frac{-\beta_3}{k_{pq}\tanh k_{pq}h - \Gamma_{pq}}, & c_{s2} &= \frac{-\beta_6}{k_{pq}\tanh k_{pq}h - \overline{\Gamma}_{pq}} \\ d_{s1} &= \frac{-\beta_4}{\overline{k}_{pq}\tanh \overline{k}_{pq}h - \Gamma_{pq}}, & d_{s2} &= \frac{-\beta_5}{\overline{k}_{pq}\tanh \overline{k}_{pq}h - \overline{\Gamma}_{pq}} \end{aligned} \right\}$$

where $\Gamma_{pp} = {\sigma_{pp}}^2/g$, $\Gamma_{pq} = {\sigma_{pq}}^2/g$, $\overline{\Gamma}_{pq} = {\overline{\sigma}_{pq}}^2/g$.

The general solutions, $\phi_{pp}^{(2)}$, $\phi_{pq}^{(2)}$ and $\phi_{pq*}^{(2)}$ in the transmitted wave region (2) are also obtained as follows:

$$\phi_{pp}^{(2)}(x,z) = B_{pp}^{(2)} Z(k_{pp}^{(2)}, z) e^{ik_{pp}^{(2)} x} + i a_{s1} \left\{ B_p^2 e^{ik_{pp} x} \right\} Z(k_{pp}, z) \tag{23}$$

$$\phi_{pq}^{(2)}(x,z) = B_{pq}^{(2)} Z(k_{pq}^{(2)}, z) e^{ik_{pq}^{(2)} x} + i c_{s1} \left\{ B_p B_q e^{ik_{pq} x} \right\} Z(k_{pq}, z) \tag{24}$$

$$\phi_{pq*}^{(2)}(x,z) = B_{pq*}^{(2)} Z(k_{pq*}^{(2)}, z) e^{ik_{pq*}^{(2)} x} + i d_{s2} \left\{ B_p \overline{B}_q e^{i\overline{k_{pq}} x} \right\} Z(\overline{k_{pq}}, z) \tag{25}$$

Green's second identity and linear equations

Potential theory shows harmonic function in a closed domain, $\phi(X)$, which is a solution of Laplace equation, can be expressed with Green's second identity

$$\phi(X) = \frac{1}{\alpha} \int_D \left\{ \phi(X_b) \frac{\partial}{\partial \nu} G(r) - G(r) \frac{\partial}{\partial \nu} \phi(X_b) \right\} ds \tag{26}$$

where $G(r) = \log r + \log r^*$, and r is the length between an arbitrary point $X = (x, z)$ in the domain and a point $X_b = (x_b,\ z_b)$ on the boundary, r^* is the length between the point X and its mirror image ${X_b}^*$ with respect to the uniform bottom boundary. α is defined to take π when X is on the boundary, and to take 2π when X is inside the boundary. ν denotes outward normal to the boundary of the region (0), and the direction of the integral is taken counterclockwise along the boundary D $(= S_1 + S_2 + S_3 + S_4)$.

By dividing the boundary D into N number of small elements, ΔS_j $(j = 1, 2, \cdots, N)$, and by assuming that the potential ϕ is uniform on each element, the integral equation (26) can be discretized as

$$\left. \begin{array}{l} \displaystyle\sum_{j=1}^{N} \left\{ \left(\overline{E}_{ij} - \delta_{ij} \right) \phi(j) - E_{ij} \frac{\partial \phi(j)}{\partial \nu} \right\} = 0 \\ \qquad\qquad (i = 1, 2, \cdots, N) \end{array} \right\} \tag{27}$$

where

$$\left. \begin{array}{ll} \displaystyle E_{ij} = \frac{1}{\alpha} \int_{\Delta S_j} G(r_{ij})\, ds, & \displaystyle \overline{E_{ij}} = \frac{1}{\alpha} \int_{\Delta S_j} \frac{\partial G(r_{ij})}{\partial \nu}\, ds \\ r_{ij} = \sqrt{(x_j - x_i)^2 + (z_j - z_i)^2}, & {r_{ij}}^* = \sqrt{(x_j - x_i)^2 + (z_j + 2h + z_i)^2} \end{array} \right\} \tag{28}$$

Substituting all the boundary conditions along the closed region (0) into equation (27), we have a set of linear equations, for the second-order as well as the first-order problems, in terms of the velocity potentials on the boundary elements and unknown coefficients A_p, B_p, A_{pp}, $B_{pp}, \cdots$. The boundary conditions on the imaginary boundaries are given through the exact solutions for $\phi_{pp}^{(2)}$, $\phi_{pq}^{(2)}$, $\phi_{pq*}^{(2)}$ in the open regions (1) and (2). Thus we solve at first the linear interaction problem (e.g., Yeoung,1975) for every component wave of angular frequency σ_p, then for every combination of the first-order solutions with frequency components σ_p and σ_q, the linear equations for the second-order potentials $\phi_{pp}^{(2)}$, $\phi_{pq}^{(2)}$, $\phi_{pq*}^{(2)}$ are solved, respectively.

Energy flux correction

The solutions have to be corrected to balance wave energy fluxes between the incident, reflected and transmitted waves, because in perturbation analysis up to the second-order the balance of wave energy flux is satisfied in the first-order; the generated second-order free waves produce excessive wave energy. The effect of this excessive energy may be negligible for a single incident wave, but for multicomponent incident wave the number of generated free waves increases in proportion to the square of the number of the incident wave components, and numerical results may become unrealistic.

To correct the numerical results so as to satisfy the conservation of the incident wave energy flux, the incident wave energy flux F_I, the reflected wave energy flux F_R and the transmitted wave energy flux F_T are calculated with numerical results of the first-order and the second-order potentials; F_R and F_T include in them the excessive wave energy flux of the generated free-waves, and thus F_I is always less than $F_R + F_T$. The correction factor β is defined as $\sqrt{F_I/(F_R + F_T)}$, and all the reflected and the transmitted wave components are multiplied by β. The effects of this energy flux correction are verified by comparing the corrected numerical results against the experimental results.

Numerical and Experimental Results

Laboratory experiments were conducted with a submerged structure as shown in figure-1 with B/h=2.0, q=0.3, R/h=0.7, and the water depth h=0.37m. Multicomponent random waves used in the experiment are shown in Table-1. For each multicomponent random wave, ten different phase combinations were used, and the results were averaged. The wave amplitudes of the component waves were set approximately the same, and for each multicomponent random wave, several different wave amplitudes ranging from small amplitude to large amplitude that intense wave breaking occurs on the structure were used to investigate the effects of wave breaking on the generation of the second-order free waves. In addition to the above multicomponent random waves, twenty component random wave, modeled from Bretschneider-Mitsuyasu spectra, was also used.

The wave tank is 0.3m wide, 0.5m deep and 28m long, and it is equipped at one end with a random wave generator having a function of wave absorption, and at the other end with a wave absorber. The reflection coefficients of the wave absorber were measured for several frequencies ranging kh=0.5 $\sim$ kh=3.0, and they are around 0.05 for waves kh greater than 1.0 (frequency 0.7_{Hz}). Thus the lowest frequency in the multicomponent random waves was chosen to be greater than kh=1.0 to minimize the contamination by the reflected waves from the wave absorber.

Before setting the model of the submerged obstacle in the wave tank, every multicomponent random wave was generated and it was measured by capacity-type wave gauges with sampling interval 10_{Hz} for the number of sampled data 8192, and from the data the incident wave spectra were obtained using First-Fourier-Transform(FFT). Then setting the model structure midway of the wave tank, transmitted waves were measured 3.0m behind the center of the structure, and the transmitted wave spectra were also calculated by FFT. The wave spectra for ten different phase combinations were averaged for every multicomponent random wave.

f (Hz)	kh	number of component			
		2	3	5	10
0.772	1.139			●	●
0.809	1.215		●	●	●
0.844	1.286	●	●	●	●
0.879	1.369	●	●	●	●
0.915	1.453			●	●
0.953	1.545				●
0.993	1.651				●
1.038	1.774				●
1.089	1.922				●
1.145	2.101				●

Table 1: Frequencies of multicomponent random waves

In the numerical calculations, the location of the right-hand side and the left-hand side imaginary boundaries are taken both 6h apart from the center of the obstacle. The length of the boundary element is taken 0.05h for all the elements. Incident wave amplitudes of component waves in the numerical calculation were obtained by integrating the power spectra of the incident multicomponent random waves in the experiment. The phases of the component waves are given by generating random number numerically, and thus the numerical calculation were also carried out for ten phase combinations as in the experiment for every multicomponent random wave. Water surface variations at the same location where transmitted waves were measured in the experiment were computed and their wave spectra were also obtained by using FFT with the same sampling interval and data length as in the experiment.

Figure-2 shows power spectra of the transmitted wave $S_T(f)$ for two component incident wave. $\overline{S}$ means component averaged power of the incident wave,

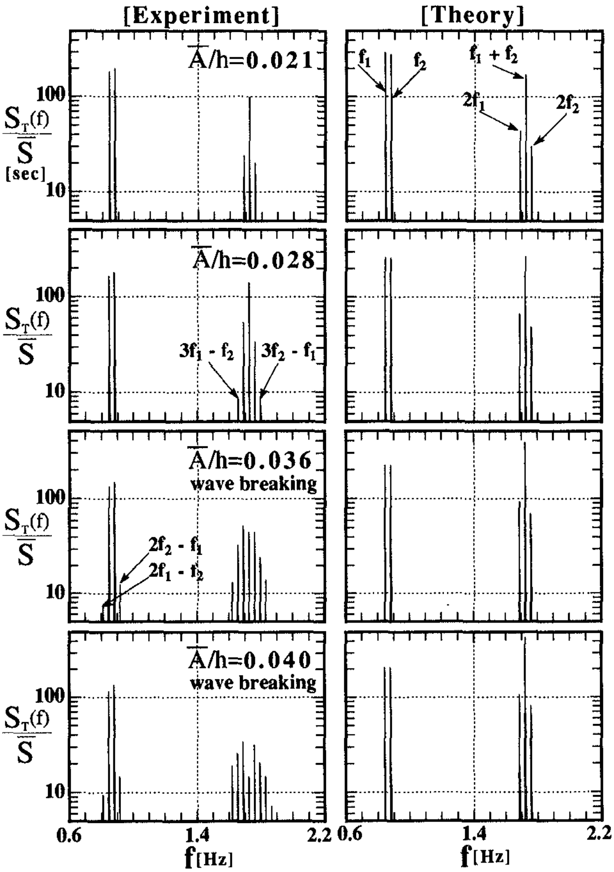

Figure 2: Comparison of the numerical results against the experimental results in terms of transmitted wave spectra $S_T(f)$ for two component wave ($f_1 = 0.772_{Hz}$, $f_2 = 0.809_{Hz}$); $\overline{S}$ is component averaged power of incident wave: from the top, figures show spectral change resulting from increase of incident wave amplitude.

which is given by dividing the power of the incident wave by its number of component. $\overline{A}$ means wave amplitude which has the same power as $\overline{S}$. Since the amplitudes of the component wave in a multicomponent random wave were made almost the same each other, $\overline{A}$ is approximately the same as the amplitude of the component wave in the experiment. In the figure-2, when the averaged wave amplitude $\overline{A}/h$ is 0.036 and 0.040, wave breakings occur on the structure, and especially when $\overline{A}/h = 0.040$ the wave breaking is very intense. The power of the second-order difference frequency waves and the power of the higher order waves generated around the third-order sum frequencies are negli-

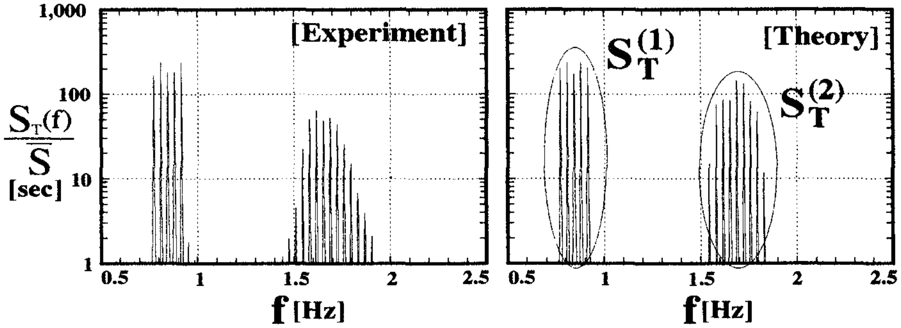

Figure 3: Comparison of the numerical results against the experimental results in terms of transmitted wave spectra $S_T(f)$ for five component incident wave: $\overline{A}/h = 0.015$.

gibly small compared to the powers of the second-order sum frequency waves, and thus results are shown for the first-order frequency and the second-order sum frequency ranges.

It can be seen that as $\overline{A}$ increases more higher order waves are observed around the second-order sum frequencies, though their powers are very small, even before wave breaking occurs. Once wave breaking occurs on the obstacle, more power is transformed to higher order waves around the incident wave frequencies (f_1, f_2) as well as around the second-order sum frequencies, and the power of the second-order sum frequency components ($2f_1$, $f_1 + f_2$, $2f_2$) decrease drastically. On the contrary in the numerical results, the amplitudes of the second-order sum frequency waves increase unrealistically even after wave breaking occurs.

The figure-3 shows the comparison for five component wave. The averaged wave amplitude $\overline{A}/h$ is 0.015 and wave breaking occurs on the obstacle intermittently. Since the energy dissipation caused by vortices and wave breaking are not considered in the present method, the numerical results gives smaller power spectra, but it can be however said that the numerical calculation gives good estimation for the spectral structure of the transmitted waves.

In order to compare the numerical results against the experimental ones more quantitatively, the power along the incident wave frequency range $S_T^{(1)}$ and the power of the second-order sum frequency range $S_T^{(2)}$ were obtained by integrating the transmitted wave spectra as illustrated in figure-3. The square root of their ratios to the power of the incident wave spectra, $\sqrt{S_T^{(1)}/S_I}$ and $\sqrt{S_T^{(2)}/S_I}$, are computed and they are shown in figure-4 for five and ten component waves. The broken lines in the figures show the numerical results without energy flux correction. The numerical results always underestimate the exper-

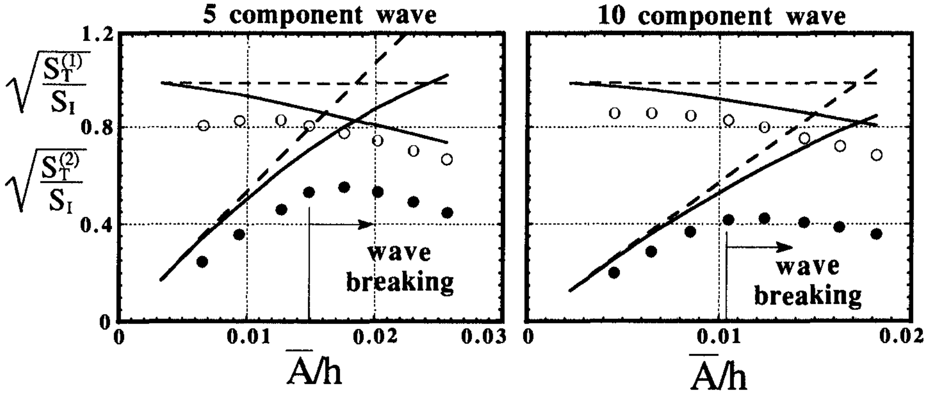

Figure 4: Comparison of the numerical results against the experimental results in terms of power $S_T^{(1)}$ obtained by integrating transmitted wave spectra along the first-order frequency range and Power $S_T^{(2)}$ for the second-order sum frequency range, which are normalized by power of incident wave S_I: ● ○ experimental results, ——numerical results with energy flux correction, - - - - - numerical result without energy flux correction.

imental results even before wave breaking occurs, due to the energy dissipation by vortices caused around the structure, and thus the numerical results gradually deviate from the experimental results as the incident wave amplitude increases. Once however wave breaking begins to occur on the structure, even it is not so intense, numerical results for the second-order waves largely underestimate the experimental results. It however should be noted that the power of the first-order frequency range $\sqrt{S_T^{(1)}/S_I}$ well estimated by the present method even after wave breaking occurs. This may imply that the energy lost by wave breaking is approximately equal to the energy which should have been transferred to the second-order free-waves in potential theory.

To show more clearly the effect of wave breaking, the ratios of $\sqrt{S_T^{(2)}/S_T^{(1)}}$ are calculated and the results are shown in figure-5. These show that the present method can well estimate the rate of wave energy transferred to the generated second-order waves as far as no wave breaking occurs on the structure.

Figure-6 shows transmitted wave spectra for twenty component incident wave, modeled of Bretschneider-Mitsuyasu spectra with significant wave height $H_{1/3} = 4.0cm$ ($H/h = 0.11$) and significant wave period $T_{1/3} = 1.25sec$ ($kh = 1.16$). No wave breaking observed in this case. Because of the energy dissipation due to vortices around the structure the numerical results underestimate the experimental ones, but overall structure of the transmitted wave spectra is well estimated.

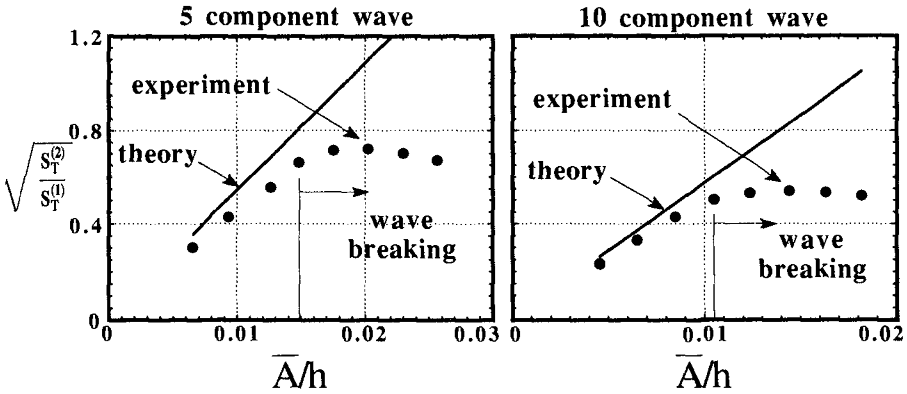

Figure 5: Comparison of the numerical results against the experimental results in terms of ratio $\sqrt{S_T^{(2)}/S_T^{(1)}}$: ——- numerical results, ● experimental results.

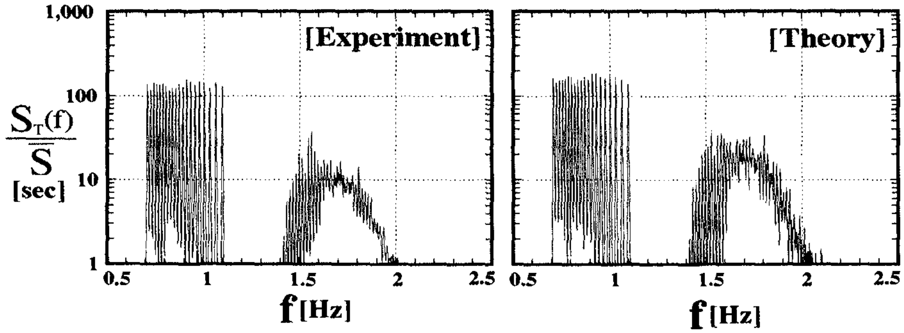

Figure 6: Comparison of the numerical results against the experimental results in terms of transmitted wave spectra for incident random wave modeled from Bretschneider-Mitsuyasu spectra ($H_{1/3} = 4cm$, $T_{1/3} = 1.25sec$); low frequency side ($f < 0.7_{Hz}$) and high frequency side ($f > 1.1_{Hz}$) are cut off in the incident wave to avoid contamination by reflected waves from wave absorber and to avoid overlap of incident wave and generated second-order sum frequency waves.

Conclusions

A numerical method to solve the second-order interactions between multicomponent random wave and submerged obstacle is presented. Numerical results give good estimation of the transformation of the incident wave spectra, caused by the second-order wave structure interactions, as long as no wave breaking occurs on the obstacle. Once however wave breaking occurs (even it is not so intense), the generation of the second-order free waves is greatly suppressed, and numerical results largely underestimate the experimental results. The energy flux correction of the numerical results is particularly effective, even after wave breaking occurs, for accurate estimation of the first-order transmitted waves.

References

Bryant, P. J.(1973): Periodic waves in shallow water, J. Fluid Mech. 59, part4, pp.625-644.

Kojim, H., A. Yoshida and T. Ijima(1994): Second-order interactions between water waves and a submerged horizontal plate, Coastal Engineering in Japan, vol.37, No.2, pp.153-172.

Massel, S. R.(1983): Harmonic generation by waves propagating over a submerged step, Coastal Engineering, Vol.7, pp.357-380.

Mei, C. C.(1983): The applied dynamics of ocean surface waves, A Wiley-Interscience Publication.

Newman, J. N.(1977): Marine Hydrodynamics, The MIT Press

Ohyama, T. and K. Nadaoka(1992): Modeling the transformation of nonlinear waves passing over a submerged dike, Proc. 23rd Coastal Eng. Conf.,pp.526-539.

Yeoung, R. W.(1975): A hybrid integral-equation method for time-harmonic free-surface flow, Proc. First Int. Conf. on Numerical Ship Hydrodynamics, pp.581-605.

Yoshida, A., K. Murakami and T. Takahira(1994): Nonlinear interaction between two component Stokes' waves and structures, Proc. of the 41th Japanese Conf. on Coastal Eng., pp.736-740.(in Japanese)